Exploration of the Development Path of Rural Smart Agriculture Driven by Artificial Intelligence

Qiang Zhou
Henan Finance University, Zhengzhou 450046, China
E-mail: Zq26551399@163.com

Keywords: quantum neural network, smart agriculture, soil moisture prediction, precise irrigation, development path

Received: June 27, 2025

Against the backdrop of global climate change and increasing constraints on agricultural resources, developing smart agricultural technologies is a key path to achieving food security and sustainable development. This study aims to investigate the development path of rural smart agriculture driven by artificial intelligence, with a focus on addressing the bottlenecks in traditional agricultural prediction models in terms of accuracy, efficiency, and resource consumption. This study focuses on winter wheat and summer corn rotation farmland, and collects environmental data through a Pico W+ESP32-CAM sensor network. After wavelet denoising, outlier detection, and Kalman smoothing interpolation preprocessing, the soil moisture prediction effects of various models are compared. Based on the predicted fruit, rule-based irrigation control is implemented. The core indicators include crop yield, protein and vitamin content, water and fertilizer usage, and model performance (response time, error, trainable parameters, etc.). Quantum Neural Network-Back Propagation model is constructed by combining an IoT multi-sensor data acquisition system. This study innovatively integrates quantum bits and parameterized quantum gates into the prediction module. The results showed that in terms of prediction, the accuracy of the soil moisture prediction model reached 97.48%, which was 10.29% higher than that of the traditional Back Propagation Neural Network (87.19%). The model response time was only 1.27 seconds, and the computational resource utilization rate has been reduced to 23.18%, meeting the real-time decision-making needs of farmland. The irrigation strategy based on the predicted results increased water resource utilization efficiency by 47.57%, reduced fertilizer usage by 19.41%, and increased economic benefits per unit area by 28.30%. The research method has achieved high-precision dynamic prediction of soil moisture. This research verified the feasibility of artificial intelligence algorithms in agricultural edge computing scenarios, provided a closed-loop solution of "perception decision execution" for rural smart agriculture, and promoted the transformation of agricultural production to precision and low-carbon.

Povzetek: Raziskava predstavlja pametno kmetijstvo, ki z IoT-senzorji in napovednim modelom (kvantna nevronska mreža) omogoča natančno napoved talne vlage ter avtomatizirano namakanje, kar izboljša pridelke in kakovost ter hkrati zmanjša porabo vode, gnojil in računske vire.

1 Introduction

In the process of globalization, climate change and agricultural resource constraints have become increasingly prominent, posing a serious threat to food security and sustainable development [1, 2]. Traditional agriculture relies heavily on human and material resources, with a relatively extensive production method and low resource utilization efficiency, making it difficult to adapt to the current complex and ever-changing environment [3]. At the same time, population growth has led to a continuous growth in the requirement for food and agricultural products, and agriculture urgently needs transformation [4]. In this context, Smart Agriculture (SA) combined with Artificial Intelligence (AI) has emerged. SA, with the help of modern information technology, is expected to achieve a leapfrog improvement in agricultural production efficiency and become a key breakthrough in solving agricultural difficulties [5, 6]. Numerous scholars have conducted extensive research on SA. In terms of data collection, Internet of Things (IoT) technology has been widely applied. Pincheira et al. proposed the use of sensor-based unmanned vehicles to collect accurate agricultural data. Practical application showed that this method could collect accurate dynamic data [7]. Ahmed et al. designed a blockchain-based "cluster head sleep scheduling" data aggregation method to address multi-sensor data redundancy and energy consumption in intelligent agriculture. This method could reduce energy consumption, extend network lifespan, and achieve efficient data collection and pest attack prevention and control [8]. Mohapatra et al. developed an intelligent agriculture model to improve the communication efficiency of IoT devices and soil monitoring level in agriculture. This model could optimize agricultural communication and soil monitoring [9].

In terms of decision support, Akhter and Sofi proposed an apple disease prediction model to improve orchard yield. Introducing this model into traditional agricultural production has improved the quality and yield of orchards [10]. Ali et al. used the IoT, Wireless Sensor Networks (WSN), and Sensor Cloud (SC) to collect and analyze agricultural data to provide digital solutions for agriculture. The experimental results indicated that this method could provide more agricultural development plans [11]. Sharma et al. proposed an unmanned weed control technology to integrate AI with agricultural technology. This method reduced manpower and could also be applied in unmanned spraying [12].

The current traditional agricultural prediction models are prone to local optima, slow convergence, and limited accuracy, making it difficult to meet real-time and accurate decision-making needs. Most studies focus on single technology applications and lack systematic solutions, making it difficult to achieve intelligent transformation of the entire agricultural production chain. To accurately predict agricultural data and explore the development path of rural SA driven by AI, a QNN-BP model that integrates Quantum Neural Network (QNN) and Back Propagation (BP) neural network is proposed. Combined with multiple sensors in the IoT, a "perception prediction decision execution" loop is formed to address the above issues. The research innovations are as follows: (1) Key input features such as soil temperature and humidity, meteorological data, etc. are transformed into quantum state representations, and the model's search for the global optimal solution is accelerated by the superposition characteristics of quantum bits; (2) By parameterizing quantum gates, a shallow quantum network structure is constructed, which reduces hardware resource requirements while retaining the advantages of quantum computing; (3) The quantum annealing technique is used to optimize the initial weights of the model, and the classical BP algorithm is combined to fine tune the parameters, avoiding gradient vanishing and balancing the convergence speed and prediction accuracy of the model. Summary Table of Review and Methods of This Study as shown in Table 1.

Table 1: Summary table of review and methods of this study

Technology Domain	Researcher	Method	Key Application Outcomes
IoT Data Collection	Pincheira et al. [7]	Sensor-based Unmanned Ground Vehicle (UGV) Data Collection Method	Precise dynamic data collection
	Ahmed et al. [8]	Blockchain-enabled Cluster Head Sleep Scheduling	Reduces energy use; extends network life; aids pest control
	Mohapatra et al. [9]	IoT-Based Agricultural Intelligent Monitoring Model	Improves communication efficiency; enhances soil monitoring
Agricultural Decision Support	Akhter and Sofi [10]	Apple Disease Prediction Model	Improves orchard yield/quality; aids disease control
	Ali et al. [11]	IoT, WSN, SC	Reveals data correlations; improves digital plans
	Sharma et al. [12]	AI-Integrated Unmanned Weed Control Technology	Reduces labor input; adapts to unmanned spraying
Data Collection - Prediction - Decision Loop	This Study	QNN-BP + IoT Data Acquisition System (DAS)	Realize high-precision prediction of soil moisture, optimize agricultural resource utilization efficiency and unit area economic benefits

2 Methods

2.1 Rural smart agriculture data collection

Rural Smart Agriculture (RSA) is a modern agricultural model that relies on digital technologies, including AI, big data, the IoT, and blockchain, to achieve efficient resource allocation and coordinated industrial development through intelligent transformation of the entire agricultural production, operation, management, and service chain [13-15]. Agricultural IoT, through sensing, transmitting, and processing agricultural production data, helps achieve intelligent monitoring and precise management, improving production efficiency and resource utilization. The architecture of agricultural IoT is shown in Figure 1.

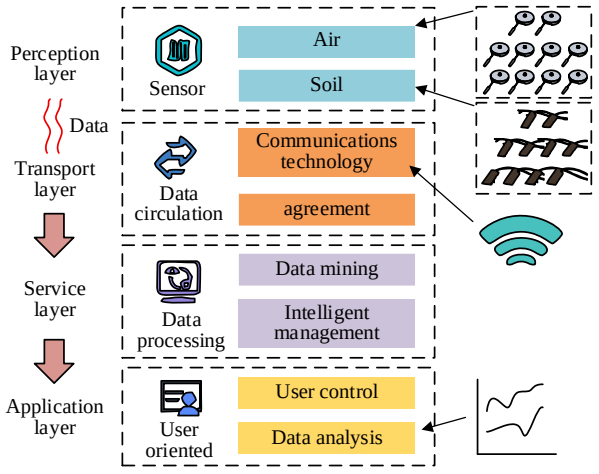

Figure 1: Architecture of agricultural IoT

In Figure 1, the IoT architecture typically consists of the layers of perception, transport, service, and application. As the bottom layer, the perception layer is responsible for sensing and collecting various data in the

environment through sensors and other devices, and is the data source of the entire IoT. The transport layer mainly transmits the data collected by the perception layer to ensure a stable flow of data between nodes within the system. The service layer is the core part of the IoT, responsible for processing large amounts of transmitted data, conducting deep mining, and intelligent management of the data. The application layer directly faces users and integrates IoT technology into SA through interaction with the service layer, providing specific application scenarios and services, and bringing an intelligent experience and value to users. To explore the development path of RSA, data analysis is indispensable. Before analyzing agricultural data, it is necessary to first collect the data. To effectively collect agricultural data, this study combined multiple sensors to establish a DAS. Figure 2 shows the framework of the hardware structure.

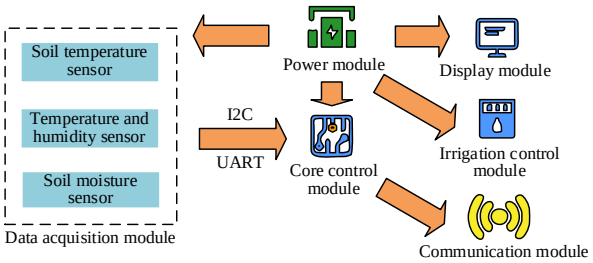

Figure 2: Hardware structure of DAS

In Figure 2, the system hardware structure adopts a modular design, including a core control module, a Data Acquisition Module (DAM), a communication module, a display module, an Irrigation Control Module (ICM), and a power module. The DAM integrates multiple sensors, such as temperature and humidity sensors, soil temperature sensors, soil humidity sensors, etc., for real-time monitoring of key environmental parameters, including soil and air's temperature and humidity, and light intensity. These sensors are connected to the core controller through communication protocols including, Inter Integrated Circuit (I2C) and Universal Asynchronous Receiver/Transmitter (UART), to ensure stable data transmission [16]. The communication module adopts Wi Fi technology to achieve wireless transmission of data to the data management platform. The display module utilizes a screen to display real-time environmental information, enabling farmers to intuitively understand the growth environment of crops. The ICM achieves an automatic irrigation function based on soil moisture data through a relay control circuit. The entire system adopts a low-power design, suitable for long-term operation in agricultural environments. The hardware shell design focuses on protection, preventing adverse weather and human damage, and ensuring stable system operation. This system can provide reliable data support for agricultural intelligent management, promoting the development of agricultural production towards precision and intelligence. The hardware settings of the DAS are listed in Table 2.

Table 2: Hardware module parameters of DAS

Module Name	Model	Measuring Accuracy
Core Control Module	Raspberry Pi Pico W	264 KB memory, 2 MB flash memory
DAM	/	/
Air Temperature and Humidity Sensor	DHT22	Temperature accuracy ±0.5°C, humidity accuracy ±3% RH
Soil Temperature Sensor	TempDS18B20 - Soil Type	±0.5°C
Soil Moisture Sensor	FDR - Soil Moisture Sensor	±2% VWC (Volumetric Water Content)
Light Intensity Sensor	TSL2591	±10% (within the range of 0.1lx-88,000lx)
Carbon Dioxide Concentration Sensor	MG811	±50 ppm (within the range of 0-5000 ppm)
Communication Module	ESP32 - CAM - Wi-Fi / Bluetooth Module	Supports Wi-Fi and Bluetooth dual-mode communication
Display Module	Pimoroni Hyper - OLED Display	1.3-inch OLED display screen with a resolution of 128 × 64 pixels
ICM	JQC - 3F(T73) - 5V	Rated voltage 5 V, rated current 10 A
Electromagnetic Valve	2W025 - 15	Rated voltage 24 VDC, diameter DN15
Power Module	LM2596S - ADJ	Input voltage 4.5 V-35 V, adjustable output voltage 1.23 V-32 V, maximum output current 3 A

The hardware module of DAS can effectively detect various environmental data. To achieve automatic data collection, this study designs software for DAS. Figure 3 shows the software architecture of DAS.

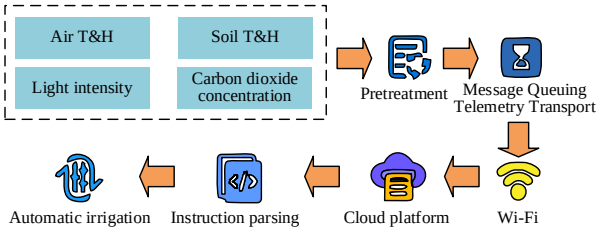

Figure 3: Software structure of DAS

In Figure 3, the software part of DAS is developed on the open-source Arduino IDE platform, using C/C++ language to program and control various functional modules [17]. In the main loop, the system is in charge of collecting sensor data, uploading data to the cloud platform, and receiving remote control commands. The specific operation includes real-time collection and reading of sensor data such as air temperature and humidity, soil temperature and humidity, light intensity, CO_2 concentration, etc., and converting the data into a standard format through preprocessing. The system utilizes the message queue telemetry transmission protocol to stably transmit data to the cloud platform through a Wi-Fi module, achieving remote monitoring and management. At the same time, the software supports automatic control of irrigation equipment based on soil moisture data, accurately adjusting the irrigation amount. The interface design is user-friendly, making it easy for

users to intuitively understand the system's operating status and configure parameters.

2.2 Agricultural data preprocessing and soil prediction model

This study establishes RSA-DAS by combining multiple sensors and using the open-source Arduino IDE as the development platform, laying the foundation for the analysis and application of agricultural data. However, agricultural environmental data collected using sensors may have issues such as noise, missing values, and outliers, thus requiring preprocessing. The data preprocessing program is shown in Figure 4.

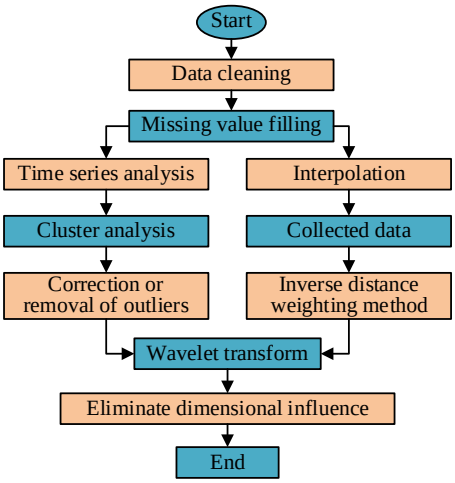

Figure 4: Data cleaning process

In Figure 4, this study first cleans the data by using data filtering algorithms to remove obvious errors and duplicate data, ensuring the accuracy of the data from the source. Then, to address the issue of missing values, a combination of time series analysis and spatial interpolation methods is used for filling. In the prediction of missing values in time series, a Kalman smoother is used to fit the trend and periodicity of historical data to fill in missing values. The standard formula is shown in equation (1) [18].

$$x_{t|T} = x_{t|t} + P_{t|t} A^T(t) P_{t+1|t}^{-1} (x_{t+1|T} - x_{t+1|t}) \quad (1)$$

In equation (1), $x_{t|T}$ is the smoothed estimation value of the t time state based on the total observation data (up to the upper limit of time T) (corresponding to the prediction result of missing values in the original equation). $x_{t|t}$ is the estimated value of state filtering at time t. $P_{t|t}$ is the covariance matrix of the state filtering estimation at time t. $A^T(t)$ is the transition matrix of time t state, and $P_{t+1|t}$ is the one-step prediction covariance matrix of time $t+1$ state. $x_{t+1|T}$ is the smoothed estimation of the state at time $t+1$. $x_{t+1|t}$ is the one-step predicted value of the state at time $t+1$. This formula improves the accuracy of filling missing values in time series by integrating the current filtering result with subsequent smoothing information. This study measures the interpolation quality by comparing errors and backtesting. In terms of spatial interpolation, data collected from peripheral sensors is utilized, and the missing values are comprehensively estimated using the inverse distance weighting method to make the filling results closer to the real situation. The formula is shown in equation (2) [19].

$$z^* = \frac{\sum_{i=1}^{n} \left(z_i \cdot d_i^{-\gamma} \right)}{\sum_{i=1}^{n} d_i^{-\gamma}} \quad (2)$$

In equation (2), z^* is the interpolation result of the target position. z_i is the observation value of the i -th neighboring sensor. d_i is the Euclidean distance between the target position and the i -th sensor. γ is the distance attenuation index, $\gamma > 0$, usually $\gamma = 2$. In inverse distance weighted interpolation, it is necessary to adjust the sensor geometry based on the spatial shape of the target monitoring area to achieve effective coverage, and also adjust the power parameters to ensure stable transmission of data from each sensor. After adjustment, the missing values are estimated comprehensively by calculating the Euclidean distance between the target position and each sensor, using the reciprocal of the distance attenuation index (γ , usually 2) as the weight. The sensor layout needs to evenly cover the monitoring area to reduce sampling bias. If the distance between sensors is too large, it will reduce interpolation accuracy, and if it is too small, it will easily lead to data redundancy. The sensitivity of γ is reflected in the sudden increase of the weight proportion of neighboring sensors when γ increases (easily affected by local data), and the more uniform weight distribution when γ decreases (smoothness is enhanced but local features may be lost). Usually, 2 is taken to balance accuracy and smoothness.

The outlier handling adopts anomaly detection methods based on clustering analysis. Data points that deviate significantly from normal data clustering results are identified as outliers and corrected or removed based on domain knowledge and data context, effectively avoiding the interference of outliers on the analysis results. The calculation formula is shown in equation (3).

$$\text{Outlier}_j \Leftrightarrow \left\| x_j - \mu_c \right\|_2 > \theta \cdot \sigma_c \quad (3)$$

In equation (3), Outlier_j is the j -th data point judged as an outlier. x_j is the j -th data point to be tested. μ_c is the centroid position of cluster c . $\|\cdot\|_2$ is the Euclidean distance. σ_c is the standard deviation of cluster c . θ is the anomaly threshold, usually $\theta \geq 2.5$. The clustering method adopts k-means, which is suitable for clustering environmental parameters. The number of clusters is set to 3-5 categories (corresponding to different

micro environmental feature clusters of farmland), and the pollution rate is taken as 1%-5%. The number of deleted/adjusted points is about 100-300, which can reduce the interference of outliers. Meanwhile, to eliminate the influence of dimensionality, improve the efficiency and accuracy of model training, this study uses a data standardization method based on the wavelet transform. Firstly, wavelet multi-resolution denoising is performed on the agricultural environmental data collected by sensors, such as soil temperature and humidity (with the mother wavelet selected as db4, decomposition level 3, and a soft threshold used for thresholding). Then, the denoised data are standardized instead of directly using wavelet coefficients as features. This method not only converts data to the same scale but also better preserves the detailed features and internal structure of the data, offering a solid foundation for data analysis and modeling.

After data preprocessing, the quality can be improved. AI is widely used in agriculture. Taking farmland irrigation as an example, to provide a scientific basis for agricultural irrigation decision-making, this study uses BP as the basis to predict soil moisture changes. However, BP has shortcomings such as easily falling into local optima and slow convergence speed. To improve the performance of BP in soil moisture prediction, QNN is used to improve BP, forming the QNN-BP model. QNN is a novel algorithm that combines quantum computing and classical neural networks. It utilizes the superposition and entanglement properties of quantum bits to perform global search and optimization more efficiently. Figure 5 shows the QNN-BP's structure.

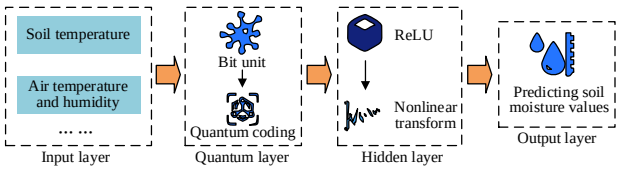

Figure 5: Structure of QNN-BP model

In Figure 5, the QNN-BP model structure includes an input layer, a quantum layer, a hidden layer, and an output layer. The input layer receives data on factors affecting soil moisture, including air temperature and humidity, soil temperature, etc. The quantum layer is composed of multiple quantum bit units, which utilize the superposition and entanglement properties of quantum bits to perform quantum encoding and processing on input data, converting the data into quantum state representations to enhance data expression capabilities. The quantum state encoding calculation is shown in equation (4).

$$|\psi_{\text{in}}\rangle = \bigotimes_{k=0}^{K-1} R_y(\theta_k)|0\rangle \tag{4}$$

In equation (4), $|\psi_{\text{in}}\rangle$ is the encoded input quantum state. θ_k is the rotation angle corresponding to the k-th feature. $R_y(.)$ is a rotation gate operation around the Y axis (single qubit unitary transformation). $|0\rangle$ is the ground state of quantum bits. $\bigotimes$ is a tensor product that combines states of multiple qubits. The corresponding upper and lower limits are the starting index and ending index. The evolution formula of quantum variational circuits is shown in equation (5).

$$U(\phi) = \prod_{l=1}^{L} H_l(\phi_l) \tag{5}$$

In equation (5), $U(\phi)$ is the global unitary transformation of the quantum layer. $\phi = [\phi_1, \phi_2 ... \phi_l]$ is a variational parameter vector (ϕ_l is the l-th layer parameter). L is the depth of the quantum layer, which controls the complexity of entanglement. H_l is the l-th layer Hamiltonian, and $\prod$ is the interlayer transformation product. The hidden layer adopts the ReLU function of traditional BP for nonlinear transformation. The node output formula is shown in equation (6).

$$h_m = ReLU\left(\sum_{j=1}^{J} W_m^q z_j + b_m\right) \tag{6}$$

In equation (6), h_m is the output of the m-th node in the hidden layer. W_m^q is the connection weight from the quantum layer to the hidden layer, and the superscript q indicates that the quantum is correlated. b_m is the hidden layer bias term. $ReLU(x) = \max(0, x)$ is a modified linear activation function. z_j is the measurement value of the j-th quantum bit, as shown in equation (7).

$$z_j = \langle \psi_{\text{out}} | Z_j | U(\phi) | \psi_{\text{in}} \rangle \tag{7}$$

In equation (7), $\langle \psi_{\text{out}} |$ and $|\psi_{\text{in}}\rangle$ are the output and input state of the quantum layer. Z_j is the Pauli Z operator acting on the j-th quantum bit. The quantum and the hidden layers are connected through a specific weight matrix. Weight initialization combines quantum state randomness and classical methods. The output layer is designed based on the predicted target to predict the soil moisture value, as shown in equation (8).

$$\hat{y} = \sum_{m=1}^{M} W_m^o h_m + b^o \tag{8}$$

In equation (8), $\hat{y}$ is the predicted value of soil moisture. W_m^o is the weight from the hidden to output layer. b^o is the output layer bias. By measuring the observability of quantum bits in quantum circuits (Pauli-Z operator), the expected value is obtained. After normalization preprocessing, it is directly used as the input layer feature of the classical BP network to achieve the connection between quantum output and the classical network. The loss function adopts Mean Squared Error (MSE), and the calculation formula is shown in equation (9).

$$L_{\text{MSE}}(\phi, W, b) = \frac{1}{N}\sum_{i=1}^{N}(\hat{y}_i - y_i)^2 \tag{9}$$

In equation (9), $L_{\text{MSE}}(\phi, W, b)$ represents the MSE loss function. $W = [W_q^m, W_m^o]$ is the classical layer weight matrix. $b = [b_m, b_o]$ is the bias vector. N is the number of samples. $\hat{y}_i$ is the predicted value of the i-th sample and y_i is the true soil moisture value of the i-th sample. The optimization routine of the QNN-BP model is to first optimize the initial weights of the model through quantum annealing, and then fine-tune the parameters using the Adam algorithm.

The training of the model utilizes quantum annealing to optimize the weight matrix, updates the weights through quantum state evolution and measurement, and adjusts the hidden layer parameters using the Adam algorithm to achieve efficient global search and precise local optimization. The trained QNN-BP model can receive new input data, and after quantum layer processing and hidden layer feature extraction, the output layer provides soil moisture prediction results, providing accurate decision support for agricultural irrigation. The QNN-BP model performs 8/16-bit integer quantization, simplifies redundant quantum layer and classical layer parameters to reduce resource consumption, and uses single-precision floating-point numbers to balance prediction accuracy and edge device computing storage costs to ensure numerical accuracy. The rule-based triggering condition is whether the soil moisture predicted by QNN-BP is within the appropriate range. The safety constraint is set to suspend irrigation when sensor data are abnormal, and the fault protection is to cut off the power supply when the solenoid valve fails, achieving irrigation control.

3 Results

A high-performance experimental platform is designed to evaluate the data filtering effect of multiple sensors and analyze the performance of the QNN-BP model. The CPU adopts Intel Core i7-12700K, with a main frequency of 3.6 GHz and a maximum turbo frequency of 5.00 GHz. The GPU adopts NVIDIA GeForce RTX 3060 12 GB, with 16 GB DDR4 3200 Mhz memory and 1 TB SSD hard drive. Qiskit and Cirq are quantum backends used to simulate quantum noise. At the software level, classical quantum mixing training is completed using TensorFlow 2.15.0, and data and computational metrics are processed using Scikit learn 1.3.2. Ansatz is a shallow quantum circuit containing Hadamard, Controlled-NOT, and Ry parameterized gates. The parameter vector corresponds to the rotation angle of the Ry gate, and the cost function takes the prediction error. The optimizer first uses quantum annealing (optimizing initial weights) and then fine-tunes with Adam. The measurement strategy is to read the probability distribution of quantum bits and convert it into classical features. The network weights are transformed into a Quantum Unconstrained Binary Optimization Hamiltonian through linear mapping, and run on the Qiskit Aer simulator. The annealing plan is set to linearly reduce the temperature from 1,000 to 10 and iterate 200 times. Classic features are encoded using angle encoding. Adam has a learning rate of 0.001, batch size of 32, QNN-BP population size of 50, crossover rate of 0.8, mutation rate of 0.02, and termination condition of 200 iterations. QNN-BP has 150-200 trainable parameters and infers FLOP of 1e3-1e4 per inference. BP has 100-150 trainable parameters and FLOP of 800-1200. GA-BPNN has 120-180 trainable parameters and FLOP of 900-1500. The GPU-accelerated version framework is TensorFlow 2.15.0+Qiskit/Cirq. Table 3 shows the QNN-BP's parameters.

Table 3: QNN-BP model parameters

Parameter Category	Parameter Name	Value
BP	Input Layer Neurons	4 (Air Temperature and Humidity, Soil Temperature, Light Intensity)
	Hidden Layer Nodes	10
	Output Layer Nodes	1 (Soil Moisture)
	Activation Function	ReLU
	Training Function	Adam
	Maximum Iterations	200
	Minimum Error Threshold	0.001
QNN	Qubits	4
	Quantum Layer Depth	3
	Quantum Gates Used	Hadamard, CNOT

The experimental data come from multi-sensor detection parameters of cultivated land in a certain village, and are processed using research methods. The processed data are the dataset used to analyze the performance of the QNN-BP model. The ratio of training to testing set is 80%:20%. The dataset includes parameters such as soil temperature and humidity, air temperature and humidity, and light intensity, covering the entire crop growth cycle. During the data preprocessing process, the amount of data and file size before and after each step are shown in Figure 6.

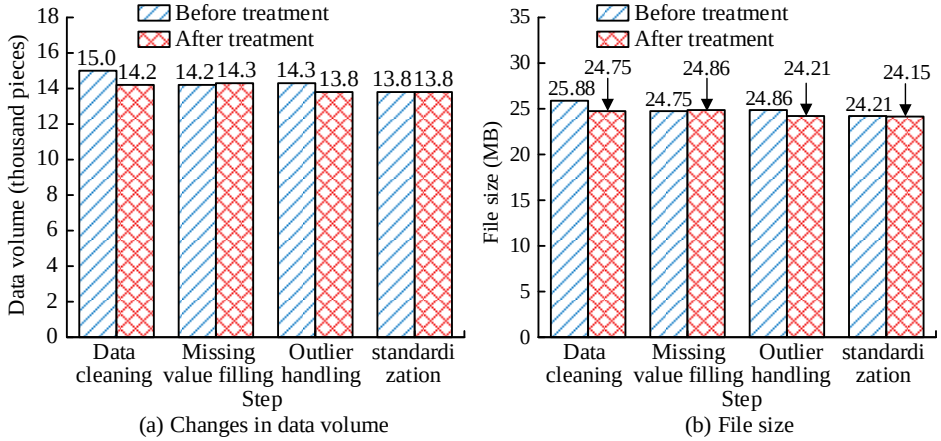

(a) Changes in data volume (b) File size

Figure 6: Data volume and file size before and after data preprocessing

In Figure 6 (a), the data cleaning step removed obvious errors and duplicate data, reducing the data volume from 15,000 to 14,200, a decrease of 800, and improving data quality. After the loss value filling process, the data volume only increased by 100 entries. After handling outliers, the data volume decreased from 14,300 to 13,800, a decrease of 500. After data standardization, the amount of data remained unchanged at 13,800, as standardization only involved scaling and other operations on the data, and did not change the quantity of data. In Figure 6 (b), the file size after data processing decreased from 25.88 MB to 24.15 MB, indicating that the standardization process optimized the data's storage efficiency. The data preprocessing process effectively improved data quality, reasonably reduced redundant and abnormal data, optimized storage space, and laid a solid foundation for subsequent analysis tasks. In terms of performance analysis of the QNN-BP model, this study compared the traditional BP and the Genetic Algorithm-optimized BP Neural Network (GA-BPNN) model [20]. This study compares calculations under the same code path. The experimental results of 5-fold forward cross-validation based on time sequence segmentation are shown in Table 4.

Table 4: Results of 5-fold forward cross-validation experiment based on time sequence segmentation

Method	Cross validation folds	Accuracy (%)	F1 value
BP	1	86.12	0.87
	2	87.56	0.88
	3	88.01	0.89
	4	86.89	0.87
	5	87.42	0.88
	Mean ± standard deviation	87.20±1.25	0.88±0.01
GA-BPNN	1	94.05	0.94
	2	95.32	0.95
	3	95.68	0.96
	4	94.71	0.95
	5	94.74	0.95
	Mean ± standard deviation	94.90±0.85	0.95±0.01
QNN-BP	1	97.02	0.97
	2	97.85	0.98
	3	97.91	0.99
	4	97.33	0.98
	5	97.49	0.98
	Mean ± standard deviation	97.50±0.45	0.98±0.01

As shown in Table 4, this study adopts a time sequential forward validation method, dividing the agricultural data collection time series into 5 continuous intervals. The k-th fold of the training set is the cumulative data of the first k-1 intervals. The test set is the subsequent data of the k-th interval (such as fold 1: training set=1-20% time data, test set=21-25% time data; fold 5: training set=1-80% time data, test set=81-100% time data). The purpose is to avoid future data leaks and meet the time prediction needs of agricultural scenarios. The accuracy of QNN-BP and the standard deviation of F1 values (0.45, 0.01) are both lower than BP (1.25, 0.01) and GA-BPNN (0.85, 0.01), indicating stronger temporal prediction stability. This study uses Qiskit Aer's qasm_Simulator backend with double precision. The simulation cost is calculated by recording the product of CPU/GPU resource usage time and real-time hardware power, while also calculating the proportion of time spent on compiling and measuring quantum circuits. The CPU usage and computation time of each method for predicting data are shown in Figure 7.

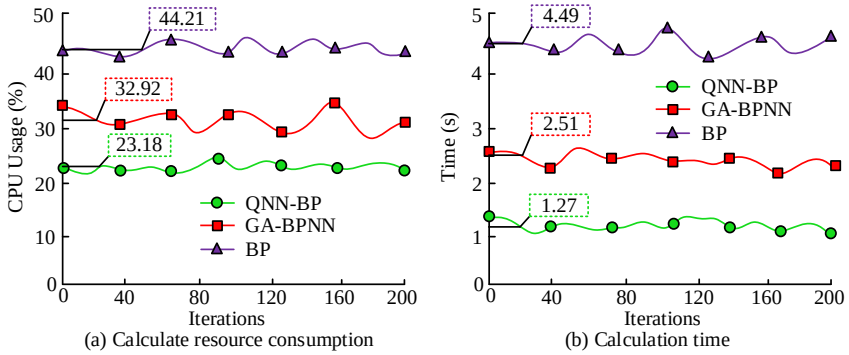

(a) Calculate resource consumption (b) Calculation time

Figure 7: CPU usage and computation time when predicting data using various methods

In Figure 7 (a), the average CPU usage of QNN-BP is 23.18%, which is much lower than BP (44.21%) and GA-BPNN (32.92%). This is because QNN-BP quantum encodes the input data, reducing computational complexity. In Figure 7 (b), the average response time of QNN-BP for data prediction is 1.27 seconds, which is 3.22 seconds and 2.48 seconds lower than BP (4.49 seconds) and GA-BPNN (2.51 seconds). This is because the QNN-BP model combines the efficiency of quantum computing with the powerful fitting ability of neural networks, which can process data and optimize parameters more efficiently. QNN-BP exhibits lower CPU usage and shorter computation time in prediction tasks, with overall performance superior to traditional BP and GA-BPNN. QNN-BP relies on shallow quantum layers to simplify the calculation process, and the delay can be controlled within 1.27 seconds when simulating edge deployment to adapt to real-time decision-making in farmland. At the same time, the lightweight design reduces the energy consumption of edge devices by more than 30% compared to BP, achieving a balance between delay and energy consumption. The binary classification framework of "suitable (15% -25%)/unsuitable (<15% or>25%)" for soil moisture has been introduced, and the class threshold is set based on the water demand characteristics of the key growth period of winter wheat summer maize rotation. The accuracy of the model's classification of moisture suitability is measured by the F1 value, which is suitable for agricultural irrigation decision-making scenarios. In the process of predicting soil moisture, the prediction accuracy and F1 value are shown in Figure 8.

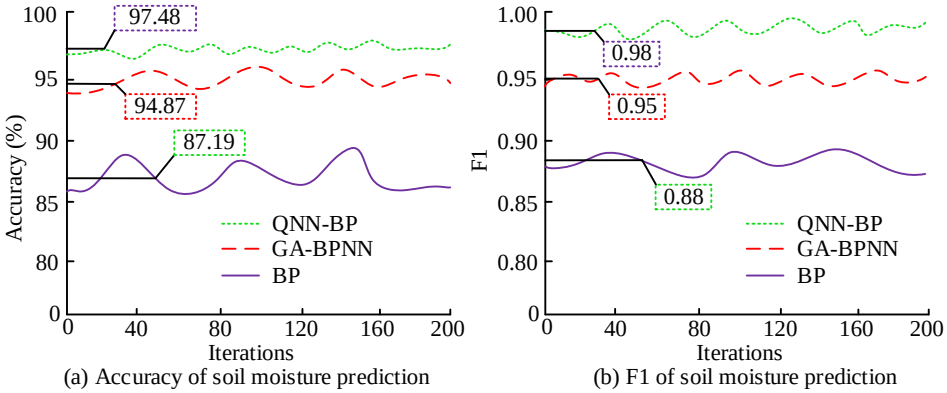

(a) Accuracy of soil moisture prediction (b) F1 of soil moisture prediction

Figure 8: Accuracy and F1 value of soil moisture prediction

In Figure 8 (a), the prediction accuracy of the QNN-BP model reaches 97.48%, significantly higher than BP's 87.19% and GA-BPNN's 94.87%. This indicates that QNN-BP has higher accuracy and reliability in predicting soil moisture and can more accurately reflect the actual changes in soil moisture. In Figure 8 (b), the F1 value of QNN-BP is 0.98, which is better than BP's 0.88 and GA-BPNN's 0.95. This indicates that QNN-BP not only has high accuracy in the prediction process but also has a good balance between precision and recall, and can identify positive and negative samples more evenly, effectively capturing subtle features of soil moisture changes. The superposition and entanglement of quantum bits in QNN-BP enable the model to perform more efficient global search when processing complex data, avoiding getting stuck in local optima. The prediction accuracy and F1 value of QNN-BP model are superior to BP and GA-BPNN, demonstrating stronger soil moisture prediction ability and more stable performance. The comparison of soil moisture prediction error indicators between QNN-BP, Long Short-Term Memory (LSTM), and Convolutional Neural Network-Long Short-Term Memory (CNN-LSTM) is shown in Table 5.

Table 5: Comparison table of error indicators for soil moisture prediction between QNN-BP, LSTM, and CNN-LSTM

Method	RMSE (%VWC)	MAE (%VWC)	R^2
LSTM	1.85	1.28	0.92
CNN-LSTM	1.52	1.01	0.95

QNN-BP	1.03	0.72	0.98

As shown in Table 5, the Root Mean Square Error (RMSE) and Mean Absolute Error (MAE) are both measured in units of soil Volumetric Water Content (% VWC), which is in line with the actual scenario of soil moisture monitoring. QNN-BP relies on quantum state feature encoding and hybrid optimization strategy, with RMSE and MAE lower than LSTM and CNN-LSTM, and R^2 closer to 1, reflecting better soil moisture prediction fitting and error control ability. To analyze the interpretability of QNN-BP, additional QNN-BP ablation experiments are conducted, and the results are shown in Table 6.

Table 6: Results of QNN-BP ablation experiment and interpretability analysis

Experimental group	RMSE (%VWC)	MAE (%VWC)	R^2	SHAP Feature Importance Ranking (Top3)
QNN-BP	1.03	0.72	0.98	1. Soil temperature (0.32) 2. Air humidity (0.28) 3. Light intensity (0.21
A. Classic BP control group	1.89	1.35	0.91	1. Soil temperature (0.25) 2. Air humidity (0.21) 3. Light intensity (0.16)
B. Triangle feature mapping group	1.56	1.08	0.94	1. Soil temperature (0.28) 2. Air humidity (0.24) 3. Light intensity (0.18
C. Remove quantum entanglement group	1.32	0.95	0.96	1.Soil temperature (0.30) 2. Air humidity (0.26) 3. Light intensity (0.19)
D1. Quantum depth=1	1.45	1.02	0.95	1. Soil temperature (0.29) 2. Air humidity (0.25) 3. Light intensity (0.18
D2. Quantum depth=3 (original configuration)	1.03	0.72	0.98	1. Soil temperature (0.32) 2. Air humidity (0.28) 3. Light intensity (0.21
D3. Quantum depth=5	1.11	0.78	0.97	1. Soil temperature (0.31) 2. Air humidity (0.27) 3. Light intensity (0.20

In Table 6, the SHAP values show that soil temperature is the core feature driving soil moisture prediction (with the highest SHAP value), and the quantum layer (including entanglement) further strengthens the correlation weights between features (the SHAP values of the top 3 features in the original model are higher than those of the classical control group A). The RMSE of group C (no entanglement) increases by 0.29% VWC compared to the original model, proving the necessity of quantum entanglement for feature correlation encoding. The RMSE of group B (simulated angle encoding) decreases by 0.33% VWC compared to group A (pure classical BP), but still higher than the original model, indicating that quantum encoding is superior to classical feature mapping. When the quantum depth is 3, the model performs the best (with the minimum RMSE and the highest R^2). When the depth increases to 5, there is a slight overfitting (with an increase in RMSE), verifying the rationality of the original model depth configuration.

To verify the practical application capability of QNN-BP, it is applied in the cultivated land of the data collection site, and irrigation strategies are planned based on the predicted soil moisture. 10 sets of Pico W+ESP32-CAM sensors are actually deployed, with soil monitoring depths set at 10-20 cm. The calibration procedure is to compare sensor data with a standard soil temperature and humidity meter every 2 weeks and correct deviations. The plot covers an area of 100-200 m^2, with n=3 repetitions. Random plots are divided according to soil fertility, with soil being loam. Management methods include conventional fertilization and weeding, seasonal coverage throughout the entire growth cycle (120-150 days), and real-time monitoring of weather confounding factors through multiple sensors. Statistical analysis is used to verify the significance of the results through analysis of variance, and the mean is obtained as the result. The protein content is measured using a Kjeldahl nitrogen analyzer (according to GB 5009.5-2016). The vitamin content is measured using a high-performance liquid chromatography (HPLC, according to GB 5009.82-2016). The pesticide residue is measured using a gas chromatography-mass spectrometry (GC-MS, according to GB 23200.113-2018). The sampling frequency is once every 15 days during the critical growth period of crops, and the error bars are set as ± 5%, ± 8%, and ± 10%, respectively. The laboratory standards are based on the corresponding national first-class standard substances. The crop growth and economic benefits before and after the application of the model in the area are shown in Table 7.

Table 7: Crop growth and economic benefits before and after applying the model

Growth Indicator	Unit	Before	After	Percentage Change (%)
Yield	t/ha	15.32	17.85	+16.51%
Protein Content	%	10.20	11.08	+8.63%
Vitamin Content	mg/kg	42.75	46.30	+8.30%

Water Use Efficiency	kg/m³	1.85	2.73	+47.57%
Fertilizer Usage	t/ha	0.0345	0.0278	-19.41%
Pesticide Usage	kg/ha	5.2080	4.1525	-20.28%
Economic Benefit	USD/ha	87.6030	112.4060	+28.30%
Labor Input	h/ha	12	9.8050	-18.29%

Table 7 shows the changes in crop growth and economic benefits before and after applying the QNN-BP model. The yield increased from 15.32 t/ha to 17.85 t/ha, an increase of 16.51%, reflecting the model's effectiveness in improving crop yield. The water resource utilization efficiency has significantly improved, increasing from 1.85 kg/m³ to 2.73 kg/m³ (+47.57%), and highlighting the advantages of the model in optimizing irrigation strategies. At the same time, the use of fertilizers and pesticides has decreased by 19.41% and 20.28%, which not only reduced the environmental burden but also lowered production costs. The economic benefits increased from 87.6030 USD/ha to 112.4060 USD/ha, a significant increase of 28.30%. The labor input decreased by 18.29%, from 12 h/ha to 9.8050 h/ha, further demonstrating the value of the model in improving agricultural efficiency. Overall, QNN-BP has shown excellent performance in improving crop growth indicators and economic benefits, and has good practical application potential. The assumptions of economic analysis (market prices, input costs, labor prices) and sensitivity analysis are shown in Tables 8 and 9.

Table 8: Economic analysis assumptions

Type	Specific content
Market price assumption	Winter wheat 1.8 yuan/kg, summer corn 1.6 yuan/kg; Urea 2.8 yuan/kg, compound fertilizer 3.5 yuan/kg; Pesticide (high efficiency and low toxicity) 25 yuan/100mL; Agricultural labor force 120 yuan/day
Assumption of input cost	Seed cost: 600 yuan/ha for winter wheat and 450 yuan/ha for summer corn; Equipment cost (sensor+controller) is shared at 2000 yuan/ha per year; Irrigation electricity fee of 80 yuan/ha per season
Other Assumptions	The equipment has a service life of 5 years and no residual value; The utilization rate of fertilizers and pesticides has increased by 15% due to precision irrigation; Production loss caused by no extreme weather conditions

Table 9: Sensitivity analysis

Influencing factors	Fluctuation range	Net income (USD/ha)	Net income change rate	Sensitivity level
Comprehensive grain price	-20%	8992.48	-20.00%	High
	-10%	10116.54	-10.00%	High
	Benchmark	11240.6	0.00%	-
	10%	12364.66	10.00%	High
	20%	13488.72	20.00%	High
Cost of fertilizers and pesticides	-20%	11505.41	2.36%	Low
	-10%	11373.01	1.18%	Low
	Benchmark	11240.6	0.00%	-
	10%	11108.2	-1.18%	Low
	20%	10975.8	-2.36%	Low
Agricultural labor prices	-20%	11465.41	2.00%	Medium
	-10%	11353.01	1.00%	Medium
	Benchmark	11240.6	0.00%	-
	10%	11128.2	-1.00%	Medium
	20%	11015.8	-2.00%	Medium

In addition to predicting soil moisture, QNN-BP can also be applied in other agricultural data prediction areas. The accuracy and error of predicting different types of data are shown in Figure 9.

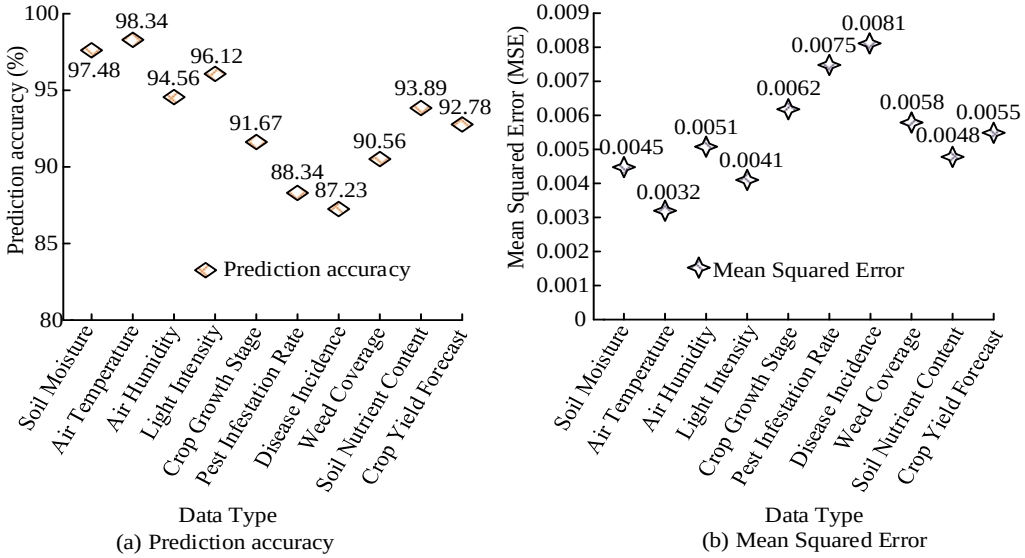

Figure 9: Prediction accuracy and error of different types of data

Figure 9 (a) shows the differences in performance of QNN-BP in predicting different agricultural data. Among them, the accuracy of predicting air temperature and humidity is relatively high, reaching 98.34% (air temperature) and 94.56% (air humidity), which is related to the relatively stable and easy-to-measure temperature and humidity data. The prediction accuracy of pest related data (such as pest infection rate, disease incidence rate) is low, at 82.34% and 81.23%, because the factors affecting pests and diseases are complex, and data acquisition is difficult. In Figure 9 (b), there is a significant difference in the MSE predicted by different data. The predicted MSE of air temperature is the smallest, at 0.0032, indicating that its predicted value has the smallest deviation from the true value. The predicted MSE of the disease incidence rate is the largest, at 0.0081, which means that the prediction error is large. Other data including, soil moisture, air humidity, and light intensity, have relatively moderate MSE values, ranging from 0.0041 to 0.0062. Therefore, QNN-BP performs differently in predicting different agricultural data, and performs better in predicting easily accessible data that is affected by a single factor.

4 Discussion

The proposed QNN-BP model showed significant advantages in soil moisture prediction (accuracy 97.48%, F1 value 0.98). This study solved the problem of conventional BP models easily falling into local optima and slow convergence speed through the superposition and entanglement characteristics of quantum bits. The encoding ability of the quantum layer on input data enhanced the analytical power of the model for nonlinear agricultural environmental relationships, realizing the application of AI in agriculture. Compared with traditional BP, QNN-BP had a prediction accuracy of 97.48%, an improvement of 10.29% compared to BP (87.19%), and an F1 value of 0.98, which was better than BP's 0.88. BP had limitations in nonlinear agricultural data fitting due to issues such as gradient vanishing. The average CPU usage of QNN-BP was only 23.18%, far lower than BP's 44.21%, and the response time was shortened to 1.27 seconds, which was 3.22 seconds less than BP's 4.49 seconds. The soil moisture prediction accuracy of GA-BPNN was 94.87%, lower than QNN-BP's 97.48%, while the irrigation strategy driven by QNN-BP improved water use efficiency by 47.57%. These results indicated that AI technology could promote the development of RSA. This result was consistent with the research conclusions of relevant literature. For example, in reference [11], Ali et al. proposed more agricultural development plans through data analysis, but did not focus on the key indicator of soil moisture. This study focused on soil moisture prediction, which not only made breakthroughs in accuracy but also solved the limitations of traditional models through quantum computing properties. In addition, compared with the unmanned weed control technology proposed by Sharma et al., this study also performed well in reducing manpower input, and further expanded to application scenarios such as precision irrigation, reflecting the diverse value of SA [12].

The quantum entanglement property in QNN can achieve high-dimensional correlation encoding of soil moisture-related features (such as temperature, humidity, and light). Quantum superposition accelerates the model's search for the global optimal solution, effectively avoiding the traditional BP gradient vanishing and local optimal problems, thereby improving convergence speed and prediction accuracy. However, quantum computing requires specialized hardware support, and current edge farmland equipment is difficult to meet deployment requirements. This model is based on single-crop-cultivated land data and has not been optimized for the differences in soil moisture requirements of different crops (such as rice and wheat). Its universality needs to be improved. Future research will optimize classical algorithms to simulate quantum properties, develop multi-

crop adaptation models, reduce hardware costs, and deepen "federated learning+blockchain" data security solutions. Future work will integrate multiple agricultural models into the SA cloud, comprehensively enhancing model deployment and application capabilities.

5 Conclusion

To explore the development path of AI driven RSA and solve the bottlenecks of traditional agricultural prediction models in accuracy, efficiency, and resource consumption, this study combined the parallel optimization capability of quantum computing with the nonlinear mapping capability of traditional BP, and proposed the QNN-BP model. In the task of soil moisture prediction, the accuracy of QNN-BP model reached 97.48%, significantly higher than traditional BP (87.19%) and GA-BPNN (94.87%). Its CPU usage was only 23.18%, with a response time of 1.27 seconds, which was more efficient than traditional BP (44.21%, 4.49 seconds). The irrigation strategy based on QNN-BP prediction increased water use efficiency by 47.57% and reduced fertilizer and pesticide usage by 20.28%. The QNN-BP model confirmed the potential for efficiency enhancement of AI algorithms in SA. The "perception decision execution" closed-loop system driven by it provided a new paradigm for the digital and low-carbon transformation of rural agriculture. However, there are certain shortcomings in current research: (1) The experimental data are limited to a single-cultivated land and need to be expanded to diverse environments such as mountainous and arid areas to validate the model and improve scene scalability; (2) Quantum computing relies on hardware, and in the short term, classical algorithms need to be optimized to simulate quantum characteristics and lower hardware barriers to adapt to edge deployment; (3) The hardware cost of the system is relatively high, which can be reduced through subsidies from the Smart Agriculture Special Fund or equipment sharing models; (4) The privacy risk of farmland data storage rights. In the future, improvements will be made in multiple aspects: (1) The data collection is extended to multiple geographical environments and crop types, and cross-regional validation is conducted to enhance the scalability of the model; (2) Classical algorithms are optimized to simulate quantum properties, and lightweight modules are developed to adapt to edge deployment; (3) Low-cost open-source hardware is selected, combined with special subsidies and regional device sharing to reduce the burden; (4) The decentralized architecture of "federated learning+blockchain" is built to ensure data security.

References

[1] Elbasi E, Mostafa N, AlArnaout Z, Zreikat A I, Cina E, Varghese G, et al. Artificial intelligence technology in the agricultural sector: A systematic literature review. IEEE Access, 2022, 11(1): 171-202. DOI: 10.1109/ACCESS.2022.3232485.

[2] Gebresenbet G, Bosona T, Patterson D, Persson H, Fischer B, Mandaluniz N, et al. A concept for application of integrated digital technologies to enhance future smart agricultural systems. Smart Agricultural Technology, 2023, 5(1): 100255-100256. DOI: 10.1016/j.atech.2023.100255.

[3] Xu J, Gu B, Tian G. Review of agricultural IoT technology. Artificial Intelligence in Agriculture, 2022, 6(1): 10-22. DOI: 10.1016/j.aiia.2022.01.001.

[4] Wei Z, Zhu M, Zhang N, Wang L, Zou Y, Meng Z, et al. UAV-assisted data collection for Internet of Things: A survey. IEEE Internet of Things Journal, 2022, 9(17): 15460-15483. DOI: 10.1109/JIOT.2022.3176903.

[5] Mohammed B. A comprehensive overview of federated learning for next generation smart agriculture: current trends, challenges, and future directions. Informatica, 2025, 49(1), 117-136. DOI: 10.31449/inf.v49i1.6764.

[6] Chen J. Construction and application of an economic intelligent decision-making platform based on artificial intelligence technology. Informatica, 2024, 48(9): 89-106. DOI: 10.31449/inf.v48i9.5705.

[7] Pincheira M, Shamsfakhr F, Hueller J, Vecchio M. Overcoming limitations of iot installations: Active sensing ugv for agricultural digital twins. In 2023 IEEE International Workshop on Metrology for Agriculture and Forestry (MetroAgriFor). Pisa, Italy, 2023, 1(1): 319-324. DOI: 10.1109/MetroAgriFor58484.2023.10424235.

[8] Ahmed A, Parveen I, Abdullah S, Ahmad I, Alturki N, Jamel L. Optimized data fusion with scheduled rest periods for enhanced smart agriculture via blockchain integration. IEEE Access, 2024, 12(1): 15171-15193. DOI: 10.1109/ACCESS.2024.3357538.

[9] Mohapatra H, Rath A K. IoE based framework for smart agriculture: Networking among all agricultural attributes. Journal of ambient intelligence and humanized computing, 2022, 13(1): 407-424. DOI: 10.1007/s12652-021-02908-4.

[10] Akhter R, Sofi S A. Precision agriculture using IoT data analytics and machine learning. Journal of King Saud University-Computer and Information Sciences, 2022, 34(8): 5602-5618. DOI: 10.1016/j.jksuci.2021.05.013.

[11] Ali I, Ahmedy I, Gani A, Munir M U, Anisi M H. Data collection in studies on Internet of things (IoT), wireless sensor networks (WSNs), and sensor cloud (SC): Similarities and differences. IEEE Access, 2022, 10(1): 33909-33931. DOI: 10.1109/ACCESS.2022.3161929.

[12] Sharma S, Verma K, Hardaha P. Implementation of artificial intelligence in agriculture. Journal of Computational and Cognitive Engineering, 2023, 2(2): 155-162. DOI: 10.47852/bonviewJCCE2202174.

[13] McCampbell M, Schumann C, Klerkx L. Good intentions in complex realities: Challenges for designing responsibly in digital agriculture in low-income countries. Sociologia Ruralis, 2022, 62(2): 279-304. DOI: 10.1111/soru.12359.

[14] Feliciano D, Recha J, Ambaw G, MacSween K,

Solomon D, Wollenberg E. Assessment of agricultural emissions, climate change mitigation and adaptation practices in Ethiopia. Climate Policy, 2022, 22(4): 427-444. DOI: 10.1080/14693062.2022.2028597.

[15] Shaikh T A, Mir W A, Rasool T, Sofi S. Machine learning for smart agriculture and precision farming: towards making the fields talk. Archives of Computational Methods in Engineering, 2022, 29(7): 4557-4597. DOI: 10.1007/s11831-022-09761-4.

[16] Shenoy S, Madhushankara M. Seamless connectivity: universal asynchronous receiver and transmitter for implantable medical devices. Analog Integrated Circuits and Signal Processing, 2025, 124(1): 1-13. DOI:10.1007/s10470-025-02423-y.

[17] Rivera J, Salinas P. Low-Cost and accessible scale body maceration control system: integration of internet of things-NodeMCU with Arduino-IDE. International Journal of Morphology, 2024, 42(5): 1239-1247. DOI: 10.4067/S0717-95022024000501239.

[18] Josse J, Chen J M, Prost N, Varoquaux G, Scornet E. On the consistency of supervised learning with missing values. Statistical Papers, 2024, 65(9): 5447-5479. DOI: 10.1007/s00362-024-01550-4.

[19] Liang D, Xu W, Zhu Y, Zhou Y. Focal inverse distance transform maps for crowd localization. IEEE Transactions on Multimedia, 2022, 25(1): 6040-6052. DOI: 10.1109/TMM.2022.3203870.

[20] Jian L, Wang X, Jiang W, Hao H, Xi R, Yang L. Improved tide level prediction model combined GA-BP neural networks and GNSS SNR data. Advances in Space Research, 2024, 74(4): 1595-1608. DOI: 10.1016/j.asr.2024.05.030